RSC Advances

ROYAL SOCIETY OF CHEMISTRY

www.rsc.org/advances

RSC Advances

ARTICLE

Photoelectrochemical properties of nanocrystalline ZnS discrete versus continuous coating of ZnO nanorods prepared by electrodeposition

Received 00th January 20xx,
Accepted 00th January 20xx

DOI: 10.1039/x0xx00000x

www.rsc.org/

A. Brayek,[a,b] S Chaguetmi,[a,c] M. Ghoul,[b] I. Ben Assaker,[b] A. Souissi,[b] L. Mouton,[a] P. Beaunier,[d] S. Nowak,[a] F. Mammeri,[a] R. Chtourou[b] and S. Ammar[a,†]

We developed nanostructured photoanodes for photoelectrochemical (PEC) water splitting and hydrogen generation. They are based on ZnO nanorods electrodeposited on a conductive ITO glass on which ZnO@ZnS heterojunction were formed using two different approaches. In a first case, the ZnO nanorods were sulfided by a prolonged contact with Na_2S aqueous solution while in the second one, they were immersed in an alcoholic solution of 2 nm sized polyol-made ZnS quantum dots (QDs). Transmission Electron microscopy showed that a continuous thin layer of ZnS is fomed around ZnO leading to a core@shell structure, in the first case, while discrete QDs agregates were grafted at the surface of these rods leading to a kind of tologyin, in the second case. PEC properties of both composite films were measured, using a home-made electrochemical cell and illuminating the anodes with a Xenon lamp. A net enhancement of the photocurrent was observed when ZnS coating was proceeded, suggesting a low carrier recombination rate and a higher efficiency toward water oxidation and then electron transfer to the used cathode (Pt wire) for H^+ reduction and H_2 generation. Interestingly, the performances of the two composite films were found to be comparable, suggesting that a discrete coating of the ZnO nanorods by a few amount of preformed ZnS QDs is enough to improve their properties for the desired application.

Introduction

Searching for novel renewable and abundant energy sources is crucial to respond to the always growing energy needs. Among the potential sources that have been investigated, hydrogen produced from photoelectrochemical (PEC) water splitting, using solar light has been gained a great deal of attention since 1972. [1] PEC is a favourable mean of converting solar energy into hydrogen since both the water and sunlight are hugely abundant. [2] It requires photoanodes, i.e. photosensitive nanostructured semiconductors, able to achieve water oxidation at their surface and to inject fresh electrons to their counter electrode, mainly Pt wire or sheet, through an external circuit, for proton reduction. [3] Numerous active wide band-gap semiconductors have been synthesized and investigated for such a purpose. The most studied are TiO_2 anatase [4] and ZnO wurtzite. [5] These oxides exhibit a suitable electronic structure regarding to the chemical potentials of the involved redox reactions. Their conduction and valence band-edges frame H_2O/H^+ and OH^-/O_2 redox levels which is absolutely required for spontaneous photo splitting of water. Focusing on ZnO oxide, 1D-morphologies such as nanorods, nanowires, nanofibers or nanotubes [6] appear to be particularly suitable for the desired application. They exhibit a high surface area and a small local electric field. In the same time, they suffer from some drawbacks limiting greatly their use at an industrial level, such as thermodynamic instabilities in electrolyte solutions (photocorrosion) and the trapping of photogenerated carriers by crystallographic lattice. Beside, despite a relatively high electron mobility, the rapid recombination of their photogenerated charge pairs contributes in reducing significantly their photoconversion efficiency. A smart way to address these limitations consists in applying a protective shell over their surface. Several hierarchical hetero-nanostructures, involving metallic and/or semiconducting nanocrystals were explored for such a purpose. [7] Recent works have shown that the formation of a ZnS shell over the ZnO surface may be very useful for such a purpose [8] and that resulting ZnO@ZnS hetero-nanostructures reach a maximum of efficiency for a potential comprised between 0 and 0.5 V (vs Ag/AgCl, pH = 7). Other works have shown that even if ZnS is a wider band-gap semiconductor compared to ZnO (3.7 eV versus 3.3 eV, respectively in their bulk form), its combination with ZnO in an optimized architecture may yield a novel material with a photo-excitation threshold energy lower than that of each component. [9]

In this context, we decided 1) to produce ZnO nanorods supported on ITO glass substrates by conventional electrodeposition route, 2) to coat them with a continuous or a discrete nanocrystalline ZnS shell and 3) to compare the photoreponse of the resulting constructs using a home-made PEC cell. Our main objective was to develop an easy-to-achieve, cheap and scalable material processing method to produce efficient hetero-nanostructures for PEC application and to determine if a discrete ZnS coating on ZnO rods is enough to enhance their PEC behaviour or if a continuous coating is absolutely necessary. In practice, the continuous coating was performed by a subsequent immersion of the as-prepared ZnO

[a] ITODYS, Univ. Paris Diderot, Sorbonne Paris Cité, CNRS UMR-7086, Paris, France.
[b] Lab. Photovoltaïque, Centre de Recherche et des Technologies de l'Energie, Technopole Borj Cedria, Hammamm Lif, Tunisia.
[c] Faculté des Sciences de Skikda, Université de Skikda, Skikda, Algeria.
[d] LRS, UPMC Univ. Paris 6, Sorbonne Universités, CNRS UMR-7197, Paris, France.
† Corresponding author: ammarmer@univ-paris-diderot.fr

nanorods in an aqueous sodium sulfide solution, while the discrete one was achieved by their impregnation in an alcoholic colloidal solution of preformed ZnS quantum dots (QDs). The produced films are designated as ZnO@ZnS-NRs/ITO and ZnO@ZnS-QDs/ITO, respectively, in the further sections. We report here their main physico-chemical properties by comparison to those of bare ZnO/ITO film, and we discuss their PEC properties with a special emphasis on the role of the ZnS coating on their photoresponse when illuminated by a simulated sunlight.

Results and discussion

A Structural and microstructural film properties

The structure of all the produced films was investigated by X-ray diffraction (XRD). All the recorded patterns are mainly indexed within the wurtzite ZnO structure (Figure 1). All exhibit the signature of ITO substrate (peaks pointed by stars) but none evidences the signature of ZnS phase, suggesting that the amount of deposited ZnS is too small to be detected by XRD and that its thickness at the extreme surface of ZnO NRs is too thin regarding the X-ray beam penetration depth.

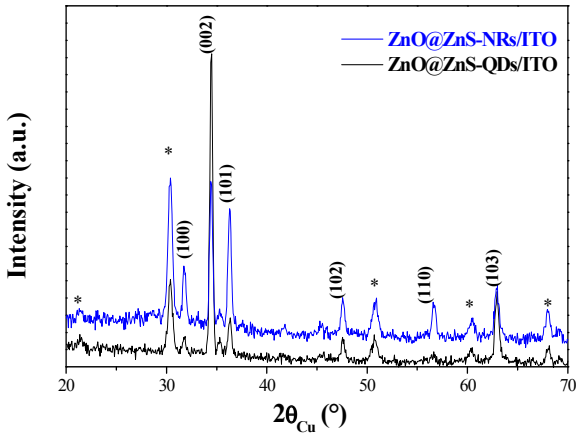

Figure 1. XRD patterns of ZnO@ZnS-NRs/ITO (blue line) and ZnO@ZnS-QDs/ITO (black line).

The refined cell parameters of the ZnO phase in all the produced samples are found to be equal to a = 3.249 Å and c = 5.206 Å, very close to those of bulk zincite (JCPDS n°79-0206), suggesting the weakness of the residual strains inferred from the ITO substrate or the ZnS coating. The highly enhanced (002) peak at 2θ = 34.40° suggests a preferential ZnO crystal growth direction along the c axis of the wurtzite lattice on ITO. It must be noticed that this preferential orientation is much more pronounced on bare ZnO (not shown) and its derivative ZnO-ZnS-QDs sample, suggesting that the chemical treatment carried out to produce ZnO-ZnS-NRs may more or less affects the crystallinity of the zincite phase.

So, to confirm ZnS coating, the surface chemical composition of both composite films was examined by X-ray photoelectron spectroscopy (XPS). The recorded survey spectra were then compared to that of ZnO/ITO film. The signature of C1s, Zn2p, O1s and S2p, at 285, 1022, 530 and 162 eV, respectively, is thus clearly evidenced in both spectra (Figure 2), while only that of C1s, Zn2p, O1s is observed in the spectrum of their parent film (not shown).

Note that Indium signal (In3d) is always present at 444 eV with an intensity as small as 1 at.-%. This result must be underlined because it agrees with an XPS analysis depth consistent with the analysis of the whole deposited ZnO layer. In other words, XPS results are representative of the chemical nature of the active part of all the prepared films.

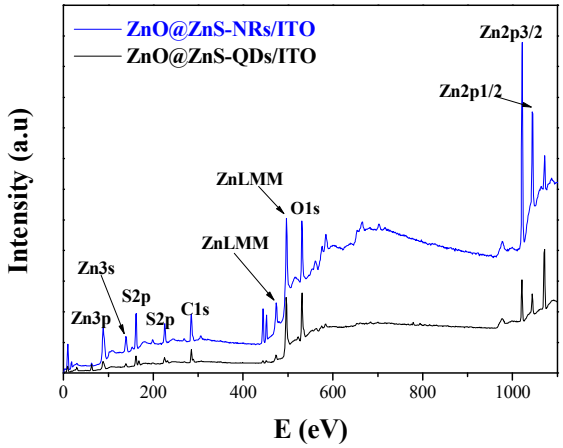

Figure 2. XPS survey spectra of ZnO@ZnS-NRs/ITO and ZnO@ZnS-QDs/ITO films. The binding energy was calibrated against the C1s adventitious carbon main peak position at 285 eV.

High resolution spectra were also recorded on the composite films in order to get new insight about the electronic states of the various elements. The accuracy of the binding energy is ± 0.1 eV. In the case of S species, S2p signal (Figure 3) is splitted into two main components of different intensities: a higher intensity peak at 162.2 eV, attributed to S^{2-}, and a lower one at 168.8 eV, usually attributed to SO_4^{2-}. Moreover, the relative intensities of these peaks are completely different between the two samples. The S^{2-} peak is significantly more intense in the ZnO@ZnS-NRs/ITO films than in the ZnO@Zns-QDs/ITO one. Altogether, these results confirm the presence of a ZnS phase at the outer surface of the produced ZnO rods, and their partial oxidation during air manipulation, the former being less oxidized than the later. A classical peak fitting of the high resolution S2p XPS spectra of the two composite films gives an oxidation ratio of 15 and 45%, respectively. According to these values, one can claim the immersion of ZnO NRs in an aqueous Na_2S solution (see experimental section) leads to the formation of an almost pure ZnS shell around them while their decoration by preformed ZnS QDs through an alcoholic impregnation route, consists in fact by grafting at their surface a kind of $ZnS@ZnSO_4$ core@shell objects. Indeed, the polyol-made ZnS nanoparticles are of 2 nm in diameter. At this size range the produced QDs become intrinsically very reactive (half of their constituting atoms forms their surface). This behaviour is quite common in chemically made nanometer-sized transition metal chalcogenide particles and does not significantly compromise their benefice toward PEC applications when they are coupled to ZnO or TiO_2 photoanodes. [10]

Zn2p high resolution XPS spectra of both composite films were also recorded (Figure 3). They consist of two main peaks related to $Zn2p_{3/2}$ and $Zn2p_{1/2}$ contributions, at about 1022 and 1045 eV,

respectively. These binding energies are slightly higher than those of pristine ZnO/ITO and those reported for bulk ZnO (Table 1). They are closest to those reported for bulk ZnS (Table 1) and for various ZnO-ZnS hetero-nanostructures, [13] evidencing Zn-S bond formation.

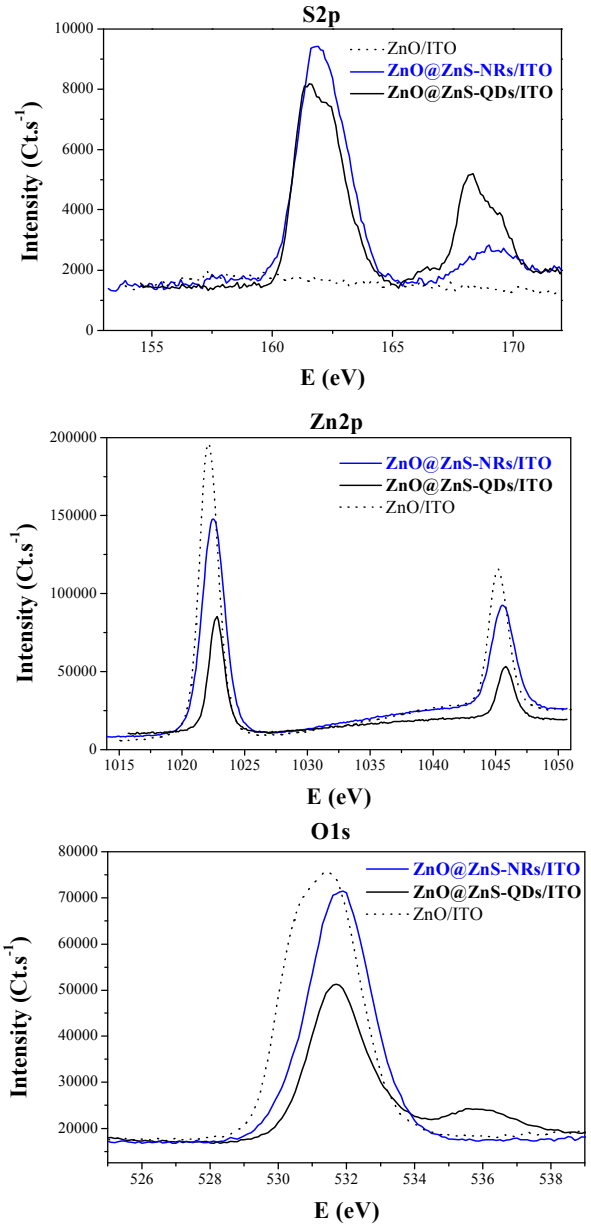

Figure 3. High resolution XPS spectra of S2p, Zn2p and O1s signals recorded on ZnO@ZnS-NRs/ITO (blue line), ZnO@ZnS-QDs/ITO films (black line) compared to those of bare ZnO/ITO (dashed line).

sample	E(FWHM) $Zn2p_{3/2}$	E(FWHM) $Zn2p_{1/2}$	Ref
ZnO/ITO	1021.7 (1.7)	1044.7 (1.7)	8a
ZnO-ZnS-NRs/ITO	1022.1 (2.1)	1045.1 (2.1)	(*)
ZnO-ZnS-QDs/ITO	1022.7 (1.5)	1045.7 (1.6)	(*)
ZnO bulk	1021.6 (1.9)	-	11
ZnS bulk	1021.9 (1.7)	1045.4 (1.7)	12

(*) this work

Table 1. Binding energy and peak width (in eV) of $Zn2p_{3/2}$ and $Zn2p_{1/2}$ signals measured on ZnO-ZnS-NRs/ITO and ZnO@ZnS-Qds/ITO films compared to those of the literature for bulk ZnO and ZnS phases.

High resolution O1s spectra of composite films were finally plotted (Figure 3). Both exhibit an intense and symmetrical peak centred at 531.9 eV, assigned to the ZnO lattice oxygen species. [14] That of ZnO-ZnS-QDs/ITO exhibit a supplementary contribution at 536.0 eV supposed to be due to sulfate species inferred from air oxidation of ZnS QDs, in agreement with previous results.

So, to have a precise idea on the morphology of the produced composite films, we recorded their scanning and transmission electron microscopy (SEM and TEM) images. The obtained SEM top view images of treated ZnO NRs on representative rods are given in Figure 4. More micrographs are given in the supplementary information section.

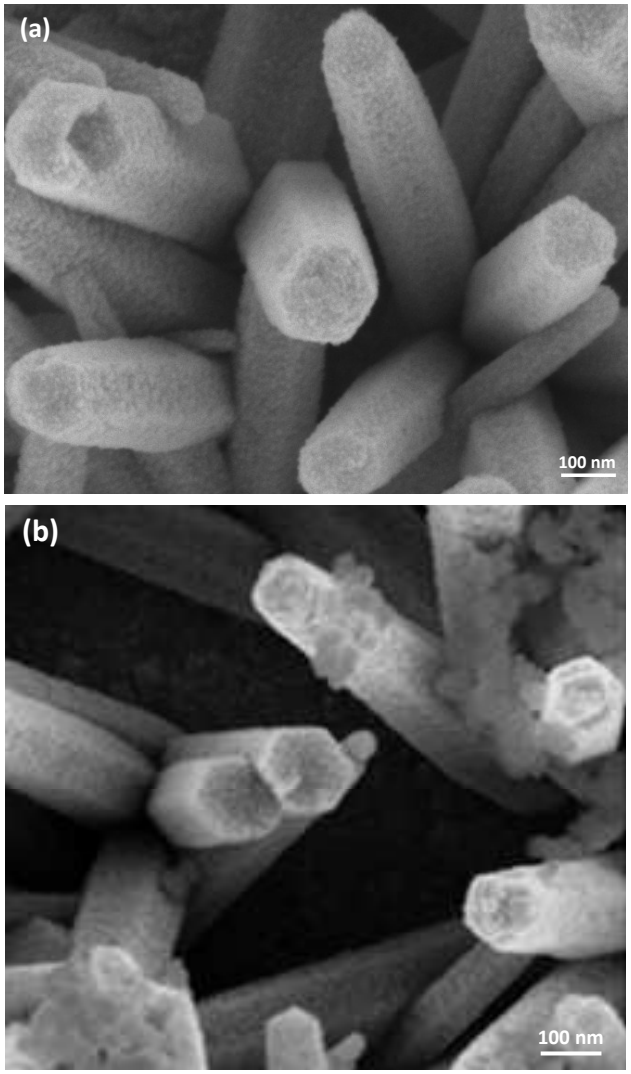

Figure 4. SEM top view of ZnO@ZnS-NRs/ITO (a) and ZnO@ZnS-QDs/ITO (b) samples.

A dense array of relatively well-aligned NRs grown on ITO substrate is clearly visible for both studied samples. In one case, NRs appear to be continuously coated by a relatively smooth and thin ZnS layer while in the other case they appear to be partially covered by ZnS nanoaggregates, in good agreement with our initial goal, namely to build continuous and discrete ZnS shell around ZnO NRs supported on a transparent and conductive sheet. TEM and high resolution (HRTEM) observations of some representative rods of the produced heterostructures are summarized in Figure 5.

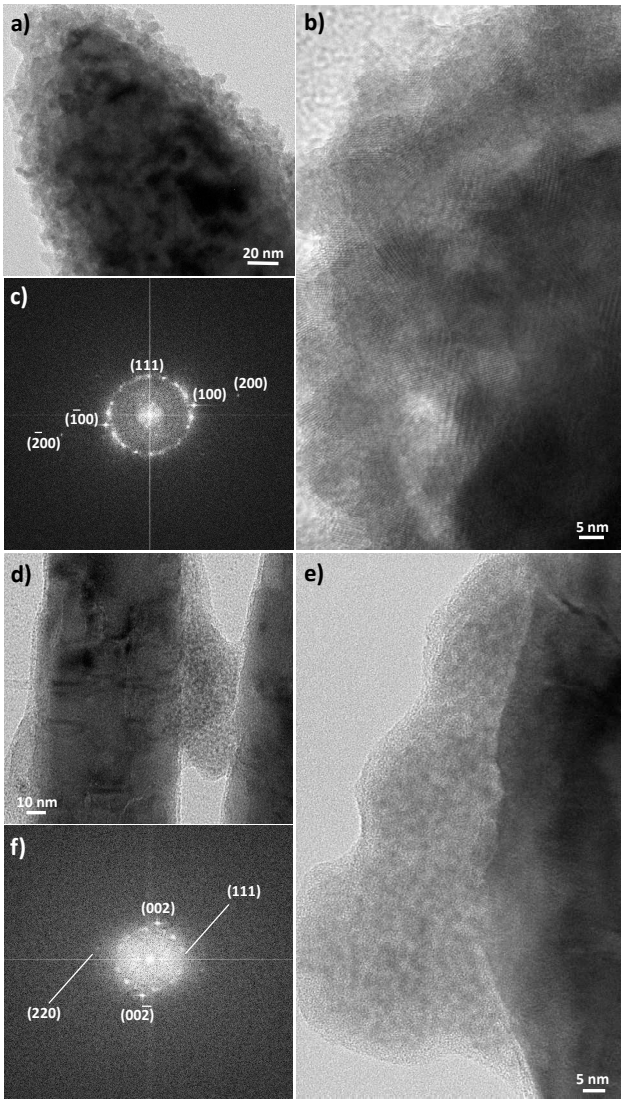

Figure 5. TEM image of a ZnO rod totally (a) or partially (d) coated, with a zoom on the coating (b and e) for ZnO@ZnS-NRs and ZnO-ZnS-QDs heterostructures, respectively. Fourrier Transforms calculated on these zones (c and f) are fully indexed within the ZnS blende structure ((111) and (220) rings) and the ZnO wurtzite one (100), (200) and (002) spots).

The outer-shell of the rods in the ZnO-ZnS-NRs/ITO sample consists of a polycrystalline continuous thin coating of 15-20 nm in thickness. The size of the crystals ranges between 5 and 8 nm and the Fourrier transform calculated from the given HRTEM image (Figure 5b) corresponds to the superposition of a Debye-Sherrer and a Laue diffractograms indexed within the ZnS blende and the ZnO wurtzite structures, respectively. Interestingly, the observed ZnO rod exposes its (100) planes, which are perpendicular to its crystallographic direction growth assumed to be parallel to the zincite c axe. In the case of the ZnO-ZnS-QDs/ITO sample, the recorded TEM micrographs show finite polycrystalline packets formed by the aggregation of tens of 2 nm-sized nanocrystals. These aggregates are of about 10 nm in thickness and 50 nm in length. They recover very partially the surface of the rods and are very often stuck between two consecutive rods. Calculating the Fourrier transform from the HRTEM images gives the same results than previously, the observed ZnO rod being exposing its (001) planes instead of the (100) ones.

Additionally, Energy Dispersive Spectrometry (EDS) analysis of the two samples was checked, focusing on the chemical composition of the border of their constituting ZnO nanorods. The obtained spectra are given in the supporting information section. They unambiguously show that the outer-shells are really consistent with a ZnS coating.

B Optical properties

In order to determine the optical band-gap energy of the composite films, their diffuse reflectance spectra were recorded in the 200-1100 nm wavelength range (not shown). The inferred optical data were then converted according Tauc relation for direct band gap semiconductors and plotted in Figure 6.

The extrapolation of the linear portion of each plot onto the energy axis gives the energy band-gap of each film. The obtained values are around 3.4 eV for both samples, comprised between that of bulk ZnO (3.3 eV) and ZnS (3.7 eV) and closer to the former concluding that the amount of ZnS is very weak at the NR surface.

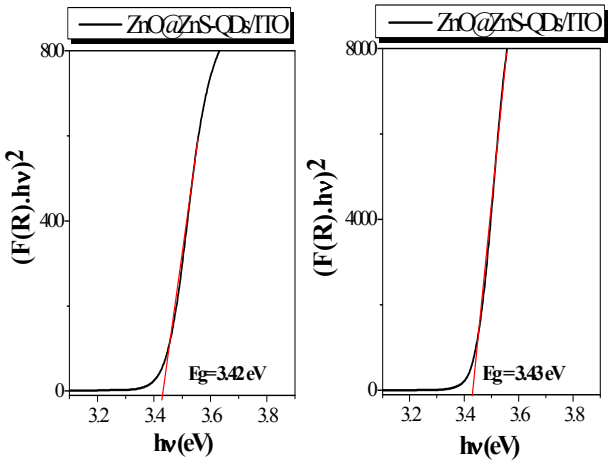

Figure 6. Tauc plots of ZnO@ZnS-NRs/ITO (left) and ZnO@ZnS-QDs/ITO (right) films as inferred from their UV-Visible diffuse reflectance spectra.

C Photo-electrochemical properties

We investigated and compared the PEC performances of both composite films to those of their ZnO/ITO parent first by cyclic voltammetry in the dark and under simulated solar light (see experimental section) (Figure 7). All the studied anodes show negligible current under dark conditions (not shown) while they exhibit an enhanced current density under illumination.

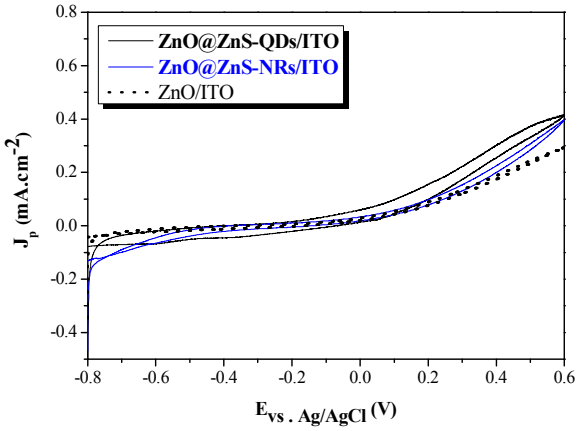

Figure 7. Photocurrent vs. potential curves plotted under simulated sunlight on ZnO@ZnS-NRs/ITO (blue line), ZnO@ZnS-QDs/ITO (solid black line) and ZnO/ITO (dashed black line) films. The potential scan rate is fixed to 10 $mV.s^{-1}$.

Interestingly, both composite films exhibit higher $J_p(E)$ values compared to bare ZnO/ITO, particularly for E as high as 0.5 V, suggesting that the built ZnO-ZnS hetero-junctions provide considerable synergy effects for enhancing charge transport and reducing recombination and trapping. [15] One can note that only slight differences exist between the $J_p(E)$ values of the two composite films.

The conversion efficiency of solar into chemical energy, η, was also calculated for different bias potentials on both composite films according the following equation: [16]

$$\eta\ (\%) = 100 \times J_p(E^\circ_{rev} - E_{app})/I_0$$

where J_p is the photocurrent density (mA cm^{-2}), I_0 is the power density of incident light (mW cm^{-2}), E°_{rev} is the standard reversible potential of 1.23 V (vs. the normal hydrogen electrode, NHE) and E_{app}, the applied potential defined as:

$$E_{app} = E_{means} - E_{oc}$$

where E_{means} is the electrode potential (vs. Ag/AgCl) of the working electrodes (the studied films) at which the photocurrent is measured under illumination and Eoc is the electrode potential (vs. Ag/AgCl) of the same electrodes in open-circuit condition (under illumination too) for the same electrolyte solution (here Na_2SO_4 0.5 M). Figure 8 shows the variation of η as a function of the potential E vs. Ag/AgCL for the two studied composite films.

The maximum of conversion efficiency, η_{max}, is obtained at 0.4 and 0.5 V for ZnO@ZnS-QDs/ITO and ZnO@ZnS-NRs/ITO films and reaches 0.26 and 0.21 % respectively. Both values are higher than that measured on bare ZnO NRs in the same operating conditions, [8a] confirming the improvement of PEC properties by coating ZnO NRs by continuous or discrete hetero-junctions with a wider band-gap II-VI semiconductor, namely ZnS. They are also of the same range order of differently prepared non-doped ZnO-ZnS 1D-hetero-nanostructures already reported in the relevant litterature. [8]

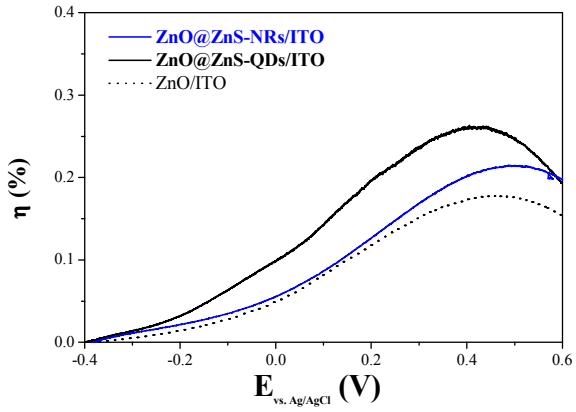

Figure 8. The photoconversion efficiency (η) curve of of ZnO@ZnS-NRs/ITO (blue line) and ZnO@ZnS-QDs/ITO (black line) films under simulated sunlight illumination (Xenon lamp), compared to that of bare ZnO/ITO.

We also measured the transient photocurrent in 0.5 M Na_2SO_4 electrolyte (pH = 7), under intermittent illumination with and without bias potential (0 and 0.5 V versus Ag/AgCl), for several cycles, to appreciate the reproducibility of the photoresponse of the prepared films (Figures 9).

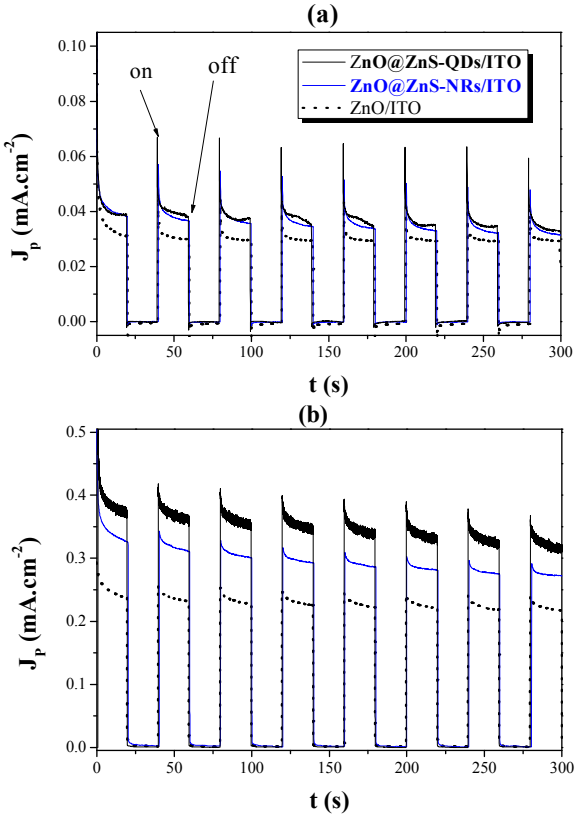

Figure 9. Photocurrent response in Na_2SO_4 aqueous solution of ZnO@ZnS-NRs/ITO (blue line) and ZnO@ZnS-QDs/ITO (black line) films under periodic Xe lamp illumination at (a) 0 and (b) 0.5 V, compared to that of their of ZnO/ITO parent (dashed line).

All the photoanodes lead to an instantaneous increase of the current upon illumination. The current retracted to the original values almost instantaneously once the illumination is switched off.

ZnS shell appear to be particularly valuable to sensitize ZnO support, increasing the measured initial photocurrent density value from a plateau value of 0.030 mA cm^{-2} for ZnO/ITO to 0.038 and 0.039 mA cm^{-2} for ZnO@ZnS-NRs/ITO and ZnO@ZnS-QDs/ITO, at 0 V. These values grow up from 0.230 to 0.300 and 0.350 mA.cm^{-2}, at 0.5 V. These results are in good agreement with previous studies wich demonstrated that the surface functionalization of ZnO by ZnS may create valuable materials for PEC applications. [8] Clearly, the continuous as well as the discrete ZnS coating allow an improved absorption of the simulated sunlight. More importantly, they promote a fast and efficient transfer of the photogenerated electrons from the ZnS shell to the ZnO cores, which leads to much reduced anodic water decomposition and greatly improved the stability of the resulting photo-devices. Indeed, in both produced composite architectures, when ZnS is illuminated, electrons transit from valence band (VB) to conduction band (CB). Since ZnS bottom CB is higher in energy than that of ZnO and since the dielectric constant of ZnS is smaller than that of ZnO, the excited electrons are immediately transferred from ZnS CB to ZnO CB. They are then ultimately transferred from bulk photoanode region to Pt electrode through the external circuit to be involved in proton reduction to form hydrogen gas. Simultaneously, vacant photo-generated holes in ZnS VB contribute to water oxidation and oxygen gas production at the surface of the photoanode. In a certain manner, fresh electrons are concentrated in ZnO CB (ZnO core) while holes are accumulated in ZnS BV (ZnS shell), before to be injected to the external circuit and used for water oxidation at the anode-electrolyte interface, respectively, as summarized hereafter:

$ZnO@ZnS + h\nu \rightarrow ZnO@ZnS(h^+, e^-)$
$ZnO@ZnS(h^+, e^-) \rightarrow ZnS(h^+)\text{-}ZnO(e^-)$
$ZnS(h^+) + H_2O \rightarrow ZnS + ½\ O_2 + 2H^+$
$ZnO(e^-) \rightarrow Pt(e^-) + ZnO$
$Pt(e^-) + 2H^+ \rightarrow Pt + H_2$

The specific band structure of ZnS assists the photogenerated holes to move faster towards the electrolyte solution to oxidize water. As a consequence, charges separation is improved and their recombination is limited, leading to higher photocurrent in the composite films. It must be underlined, that PEC improvements are almost equivalent in both architectures. In other words, decorating ZnO NRs by a few amount of preformed QDs, using an easy-to-achieve material processing route, namely impregnation, is as efficient as coating them by a continuous ZnS shell through their surface sulfidation by an immersion in a Na_2S slution.

Concerning the robustness of the built ZnO@ZnS/ITO electrodes toward photocorrosion into the electrolyte solution, compared to bare ZnO/ITO one, the results are unfortunatly less spectacular. Indeed, ZnO is known to be unstable under light illumination. Photo-induced anodic reactions usually cause Zn^{2+} ions, $Zn(OH)_4^{2-}$ and $Zn(OH)_3^-$ species injection into the electrolyte solution and hence decrease largely the photocurrent over the operating time. In the present case, the photocurrent density decreases by about 8% from its initial values along of 300 s of working time. This decrease reaches about 15% in the composite electrodes, suggesting a poorer chemical stability of ZnS compared to ZnO. The conversion of ZnO nanorods into ZnO@ZnS core-shell without scavengers in the electrolyte solution does not protect them significantly from corrosion. To the best of our knolwedge, replacing Na_2SO_4 passive electrolyte by Na_2S and/or Na_2SO_3 ones should provide stable ZnS surface. [17] In practice, sulfide and/or sulfite ions of such active electrolytes act as hole scravengers and avoid ZnS photocorrosion, [17] offering thus the possibility to overcome the ZnO@ZnS/ITO photocorrosion drawback, making the observed J_p improvement stable over the operating time.

Experimental

A Film preparation

All the reagents were of analytical grade and were used as received without further purification. All aqueous and alcoholic solutions were prepared using deionized water and absolute ethanol, respectively. ZnO NRs were first produced by electrodeposition on commercial glass sheets coated with Sn-doped polycrystalline In_2O_3 (ITO) (resistance of 10 Ωm). The sheets were immersed in an aqueous solution of $ZnCl_2$ (5.0×10^{-4} M) and KCl (1.0×10^{-1} M), under continuous bubbling of dioxygen, using a classical three-electrode electrochemical cell [18] within optimized potentiostatic conditions. [19] The resulting film consists of dense and almost well-aligned, perpendicular to the ITO surface, ZnO NRs of about 100 nm in diameter and 10 µm length (Figure 10).

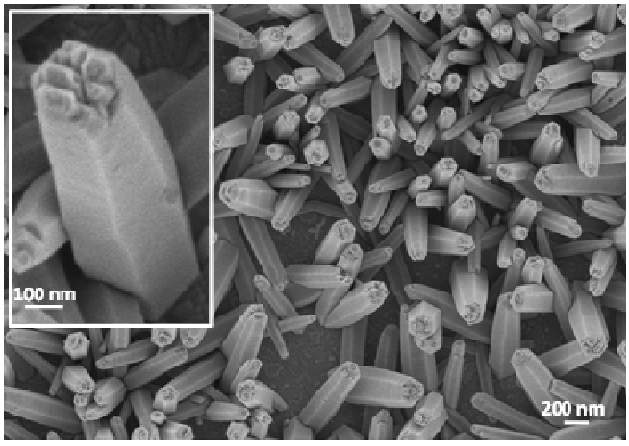

Figure 10. SEM top view image of an assembly of ZnO NRs. A zoom on a representative rod is given in the inset.

Parallel to that, ZnS QDs were synthesized using the polyol process. [20] In practice, 21.9 mg of $Zn(CH_3CO_2)_2.2H_2O$ (1.0×10^{-4} M) and 9.13 mg of thiourea (1.1×10^{-4} M) were dissolved in 80 mL of diethyleneglycol (DEG) under mechanical stirring in a flask and

heated at 180 °C (6 °C min^{-1}). The mixture was maintained for 30 min under reflux and then quickly cooled to room temperature using an ice bath. The recovered sol consists of almost isotropic monodisperse ZnS nanoparticles of about 2 nm in size (Figure 11).

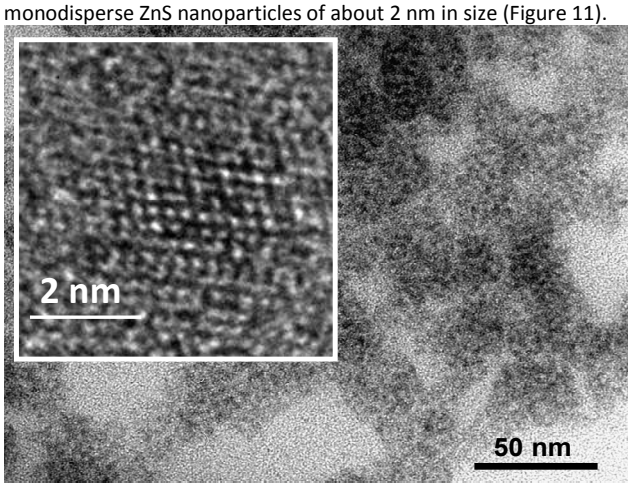

Figure 11. TEM image of an assembly of 2 nm sized polyol-made ZnS particles. In the inset an HRTEM image of one representative particle.

Continuous and discrete ZnS coating of the ZnO NRs was carried out by immersing them overnight, in an aqueous Na_2S solution (3.2×10^{-1} M), placed in a 60 °C water bath, [19] and in a DEG colloidal solution of polyol-made ZnS (QDs) diluted in ethanol (1:5), [21] respectively. In all the cases, the films were washed with water and ethanol several time before being dried at 80 °C for 12 hr. Note that after 3 washing cycles, all the carried out structural and microstructural characterizations on the resulting hybrid samples gave the same results, with particularly the same ZnS XPS signature, allowing us to fixe the number of washing cycles to 3. To summarize all the ZnS coating approaches, a recapitulative scheme is given in Figure 12.

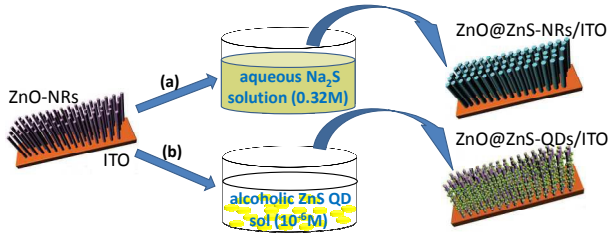

Figure 12 General scheme of ZnO NRs coating by a continuous (a) or a discrete (b) nanocrystalline ZnS shell.

B Film characterization

XRD analysis was carried out on all the produced samples using an Empyrean (PANALYTICAL) diffractometer equipped with a multichannel PIXcel 3D detector and a Cu Kα X-ray source (1.5418 Å). Typically, each pattern was recorded in grazing conditions (GIXRD) in the 20-70° 2θ range (0.026° for 297 s). To obtain a quasi-parallel beam and make measurements insensitive to sample tilt, the samples were mounted on a five-axes cradle with motorized movements to obtain a perfectly plane position. This cradle gives also the opportunity to apply a phi-rotation (around z-axis) and a psi-tilt (around x-axis). SEM and TEM were also carried out to investigate the exact morphology of the produced samples, using a Supra40 ZEISS and a JEOL JEM-100CX -II microscopes operating at 5 and 100 kV, respectively. HRTEM observations were performed on suspensions containing the nanorods, sonicated for few minutes in ethanol before deposition of few drops on copper coated carbon grids. HRTEM experiments were performed on a JEOL JEM 2010 UHR microscope operating at 200 kV. The images were collected with a 4008 X 2672 pixels CCD camera (Gatan Orius SC1000).The chemical analyses were obtained by selected energy-dispersive X-ray spectroscopy (EDS) microanalyser (PGT-IMIX PC) mounted on the microscope. XPS was performed on a Thermo VG ESCALAB 250 instrument equipped with a micro-focused, monochromatic A1 Kα X-ray source (1,486.6 eV) and a magnetic lens. The X-ray spot size was 500 µm (15 kV, 150 W). The spectra were acquired in the constant analyzer energy mode with pass energy of 150 and 40 eV for the general survey and the narrow scans, respectively. Finally, the UV-visible diffuse reflectance spectra of all the samples were recorded, in the 200-800 nm range, on a Perkin Elmer-Lambda 1050 spectrophotometer equipped with a PTFE coated integration sphere.

C Photoelectrochemical measurements

The photo-responses of all the prepared films were evaluated by measuring the photocurrent density J_p, using a VMP100 potentiostat from Bio-Logic. The measurement of the photocurrent density as a function of the applied potential E was performed in a standard three-electrode configuration (single-compartment) home-made cell. [22] The potential of each prepared sample (used as working electrode) was measured using a saturated calomel electrode (SCE), using a Pt wire as counter electrode. A solution of Na_2SO_4 (0.5 M, pH = 7) was used as electrolyte. The whole cell was purged with argon prior to all experiments. A surface of 0.7×1.0 cm^2 was illumined on each sample by a 150 W Xenon lamp (ORIEL instruments), to mimic solar light, leading thus to power density of incident light I_0 of 50 $mW.cm^{-2}$.

Conclusion

Almost vertically aligned ZnO@ZnS nanowire arrays were successfully synthesized on ITO substrate using two different routes. In a first case, ZnO nanorods were sulfurized by a prolonged contact with Na_2S aqueous solution while in the second one, they were immersed in a polyol solution of 2 nm sized polyol-made ZnS quantum dots (QDs). The photo-electrochemical performances of the resulting hetero-nanostructures appeared to be improved compared to those of their parent counterparts. Their initial photocurrent densities J_p measured on a home-made PEC cell illuminated with a standard Xenon lamp, were found to be higher than that of their parent film. We believe that when ZnS coating is proceeded, a low carrier recombination rate and a higher efficiency toward water oxidation and then electron transfer to the used cathode (Pt wire) for H^+ reduction and H_2 generation are achieved. Besides, these J_p values are comparable between the two composite films, demonstrating the excellent potential of the discontinuous ZnS coating in the design and preparation of valuable photoanodes. Noteworthy

the use of passive electrolyte, namely Na_2SO_4 aqueous solution, does not prevent ZnS photocorrosion. Its replacement by Na_2S and/or Na_2SO_3 should overcome this drawback.

Acknowledgements

The authors are indebted to B. Piro and P. Decorse (Paris Diderot University) for Photoelectrochemistry and X-ray Photoelectron Spectroscopy technical support, respectively. They are also indebted to the Tunisian Education and Research Minister for the A.B. PhD's grant.

Notes and references

1 F. Akira, H. Kenichi, *Nature*, 1972, **238**, 37.
2 O. Khaselev, J. A. Turner, *Science*, 1998, **280**, 425.
3 R. M. N Yerga, M. C. A. Galvan, F. del Valle, J. A. V. de la Mano, J. L. G Fierro. *Chem.Sus. Chem.,* 2009, **2**, 471.
4 Z. H. Zhang, M. F. Hossain, T. Takahashi, *Int. J. Hydrogen Energy*, 2010, 35, 8528; N. K. Allam, C. A. Grimes, *Langmuir*, 2009, **25**, 7234.
5 C. Perkins, P. R. Lichty, A. W. Weimer, *Int. J. Hydrogen Energy,* 2008, **33**, 499; X. Yang, A. Wolcott, G. Wang, A. Sobo, R. C. Fitzmorris, F. Qian, J. Z. Zhang, Y. Li, *NanoLett*, 2009, **9**, 2331; G. Monika, S. Vidhika, S. Jaya, S. Anjana, A. P. Singh, V. R. Satsangi, S. Dass, R. Shrivastav, *Bull. Mater Sci*., 2009, **32**, 23.
6 H. Zhao, W. Fu, H. Yang, Y. Xu, W. Zhao, Y. Zhang, H. Chen, Q. Jing, X. Qi, J. Cao, X. Hou, Y. Li, *Appl. Surface Sci.,* 2011, **257**, 8778; X. T. Zhou, P. S. G. Kim, T. K. Sham, S. T. Lee*, J. Appl. Phys.*, 2005, **98**, 024312 ; c) X. H. Sun, S. Lam, T. K. Sham, F. Heigl, A. Jurgensen, N. B. Wong, *J. Phys. Chem. B*, 2005, **109**, 3120.
7 a) H. Xia, C. Hong, X. Shi, B. Li, G. Yuan, Q. Yao, J. Xie, *J. Mater. Chem. A*, 2015, **3**, 1216 ; b) H. Xia, W. Xiong, C. K. Lim, Q. Yao, Y. Wang, J. Xie, *Nano Research*, 2014, **7**, 1797 ; c) P. Thiyagarajan, H.-J. Ahn, J.-S. Lee, J.-C. Yoon, J.-H. Jang, *Small*, 2013, **9**, 2341 ; W. Sheng, B. Sun, T. Shi, X. Tan, Z. Peng, G. Liao *ACS Nano*, 2014, **8**, 7163.
8 a) A. Brayek, S. Chaguetmi, M. Ghoul, I. Ben Assaker, A. Souissi, R. Chtourou. P. Decorse, H. Lecoq, S. Nowak, L. Mouton, F. Mammeri, S. Ammar, *J. Power Sources*, 2015, submitted ; b) J. Chung, J. Myoung, J. Oh, S. Lim, *J. Phys. Chem. C*, 2010, **114**, 21360 ; c) A. Kushwaha, M. Aslam, *Electrochim. Acta*, 2014, **130**, 222.
9 J. Lahiri, M. Batzill, *J. Phys. Chem. C*, 2008, **112**, 4304; J. Schrier, D. O. Demchenko, L. W. Wang, *NanoLett*., 2007, **7**, 2377.
10 J. S. Jang, H. G. Kim, U. A. Joshi, J. W. Jang, J. S. Lee, *J. Hydrogen Energy*, 2008, **33**, 5975.
11 S. Bera, S. Dhara, S. Velmurugan, A. K. Tyagi, *Int. J. Spectroscopy*, 2012, 371092.1; C. D. Wagner, W. M. Riggs, L. E. Davis, J. F. Moulder, G. E. Muilenberg, *Handbook of XPS*, Perkin Elmer Corporation, Eden Prairie, Minn (USA) 1979.
12 G. Wang, B. Huang, Z. Li, Z. Lou, Z. Wang, Y. Dai, M.-H. Whangbo, *Scientific Rep*., 2014, **5**, 8544.1; N. Biswal, D. P. Das, S. Martha, K. M. Parida*, Int. J. Hydrogen Energy,* 2011, **36**, 13452; J. F. Xu, W. Ji, J.Y. Lin, S.H. Tang, Y.W. Du, *Appl. Phys. A: Mater. Sci. Process.,* 1998, **66**, 639;
13 S. Dhara, K. Imakita, P. K. Giri, M. Mizuhata, M. Fujii, *J. Appl. Phys.,* 2013, **114**, 134307; H. X. Sang, X. T. Wang, C. C. Fan, F. Wang, *Int. J. Hydrogen Energy,* 2012, **37**, 1348.
14 M. Koudelka, A. Monnier, J. Sanchez, J. Augustynski, *J. Mol. Catal.,* 1984, **25**, 295 ; Q. Simon, D. Barreca, A. Gasparotto, C. Maccato, T. Montini, V. Gombac, P. Fornasiero, O. I. Lebedev, S. Turner, G. V. Tendeloo, *J. Mater. Chem.,* 2012, **22**, 11739.
15 J. Reber, K. Meier, *J. Phys. Chem*., 1984, **88**, 5903.
16 M. Zhong, Y. Li, I.Yamada, J. J. Delaunay, *Nanoscale,* 2012, **4**, 1509; H. Kim, M. Seol, J. Lee, K. Yong, *J. Phys. Chem. C,* 2011, **115**, 25429.
17 Z. Chen, T. F. Jaramillo, T. G. Deutsch, A. Kleiman-Shwarsctein, A. J. Forman, N. R. Garland, *Mater. Res.,* 2011, **25**, 3; J. Jiang, M. Wang, L. Ma, Q. Chen, L. Guo, *Int. J. Hydrogen,* 2013, **38**, 3077.
18 S. Peulon, D. Lincot, *J. Electrochem. Soc.,* 1998, **145**, 864; T. Pauporté, D. Lincot, *Electrochim. Acta*, 2000, **45**, 3345.
19 A. Brayek, M. Ghoul, A. Souissi, I. Ben Assaker, H. Lecoq, S. Nowak, S. Chaguetmi, S. Ammar, M. Oueslati, R. Chtourou, *Mater. Lett.,* 2014, **129**, 142.
20 M. Gaceur, M. Giraud, M. Hemadi, S. Nowak, K. David, J. P. Quisefit, N. Menguy, M. Boissière, S. Ammar. *J. Nanopart. Res.*, 2012, **14**, 932.
21 S. Chaguetmi, F. Mammeri, M. Gaceur, S. Nowak, P. Decorse, H. Lecoq, A. Slimane, R. Chtourou, S. Ammar, *RSC Adv*., 2013, **3**, 2572.
22 S. Chaguetmi, F. Mammeri, S. Nowak, H. Lecoq, P. Decorse, C. Costentin, S. Achour, S. Ammar, *J. Nanopart. Res*., 2013, **15**, 2140.

Photoelectrochemical properties of nanocrystalline ZnS discrete versus continuous coating of ZnO nanorods prepared by electrodeposition